Title	Proposal of multidimensional quantum walks to explore Dirac and Schr?dinger systems
Author(s)	Yamagishi, Manami; Hatano, Naomichi; Imura, Ken-Ichiro et al.
Citation	Physical Review A, 107(4), 42206 https://doi.org/10.1103/PhysRevA.107.042206
Issue Date	2023-04-10
Doc URL	https://hdl.handle.net/2115/89815
Rights	©[2023] American Physical Society
Type	journal article
File Information	PhysRevA.107.042206.pdf

Proposal of multidimensional quantum walks to explore Dirac and Schrödinger systems

Manami Yamagishi [ORCID],[1,*] Naomichi Hatano [ORCID],[2,†] Ken-Ichiro Imura [ORCID],[2,‡] and Hideaki Obuse [ORCID][3,2,§]

[1]*Department of Physics, the University of Tokyo, 5-1-5 Kashiwanoha, Kashiwa, Chiba 277-8574, Japan*
[2]*Institute of Industrial Science, the University of Tokyo, 5-1-5 Kashiwanoha, Kashiwa, Chiba 277-8574, Japan*
[3]*Department of Applied Physics, Hokkaido University, Kita 13, Nishi 8, Kita-Ku, Sapporo, Hokkaido 060-8628, Japan*

We propose a multidimensional discrete-time quantum walk (DTQW), whose continuum limit is an extended multidimensional Dirac equation, which can be further mapped to the Schrödinger equation. We show in two ways that our DTQW is an excellent measure to investigate the two-dimensional (2D) extended Dirac Hamiltonian and higher-order topological materials. First, we show that the dynamics of our DTQW resembles that of a 2D Schrödinger harmonic oscillator. Second, we find in our DTQW topological features of the extended Dirac system. By manipulating the coin operators, we can generate not only standard edge states but also corner states.

I. INTRODUCTION

The quantum walk is a quantum analog of a random walk. Instead of stochastic fluctuations of a classical random walker, a quantum walker moves under interference of quantum fluctuations at each site, which deterministically governs the walker's dynamics. The quantum walk was originally introduced by Aharonov *et al.* [1], who first referred to it as a "quantum random walk." Meyer [2] built a systematic model and found a correspondence to Feynman's path integral [3] of the Dirac equation. Starting with Farhi and Gutmann [4], quantum walks have been well studied in the context of quantum information [5,6]. To this day, studies of quantum walks have become even more interdisciplinary and extended over a variety of research fields, such as biophysics [7,8] and condensed-matter physics [9], particularly topological materials [10–12].

There are two types of time evolution: continuum-time quantum walks and discrete-time quantum walks (DTQWs). We focus on the latter, in which the space and time are both discrete. Strauch [13] showed that the continuum limit of the unitary time evolution of a one-dimensional (1D) DTQW gives that of a Dirac particle. This correspondence of DTQW has enabled us to understand the physical meaning of quantum walks better. Since squaring the Dirac Hamiltonian with a linear potential produces the Schrödinger Hamiltonian with a harmonic potential, we can make further correspondence between a quantum walker and a Schrödinger particle in 1D. However, such investigation has been limited to 1D systems. In two-dimensional (2D) systems, some quantum walks give a Dirac Hamiltonian in its continuum limit [14–16], but there

are usually only two internal states and hence one cannot obtain the 2D Schrödinger Hamiltonian by squaring it.

In this paper, we show in two ways that our DTQW is an excellent measure to investigate an extended 2D Dirac Hamiltonian with additional internal degrees of freedom. We analyze its dynamics and topological properties, especially as higher-order topological insulators [17–19]. We start with proposing a 2D extended Dirac Hamiltonian,

$$
\begin{aligned}
H_{\mathrm{D}}^{(2)} &:= H_{\mathrm{D}_x} \otimes \tau^0 + \sigma^x \otimes H_{\mathrm{D}_y} \\
&:= [\epsilon \sigma^z p_x + m_x(x)\sigma^y] \otimes \tau^0 + \sigma^x \otimes [\epsilon \tau^z p_y + m_y(y)\tau^y].
\end{aligned}
\tag{1}
$$

that can be mapped to a 2D DTQW as well as to a Schrödinger Hamiltonian, as we will show below. Our key trick is to introduce σ^x in the second term so that upon squaring the Hamiltonian (1) all crossing terms may vanish and the result can be the standard 2D Schrödinger Hamiltonian. With the additional internal degrees of freedom due to the introduction of σ^x, we refer to the Dirac Hamiltonian (1) as the extended Dirac Hamiltonian. The same applies to higher-dimensional cases; see Eq. (15) below for the three-dimensional (3D) case with an eight-dimensional internal degree of freedom.

Remember that the original 3D Dirac equation is written with a four-dimensional spinor degree of freedom, which Dirac assigned to a particle and an antiparticle each with a spin $1/2$ degree of freedom. This is partly because the four-dimensional degree of freedom is the minimal representation of gamma matrices that satisfies the anticommutation relation necessary in deriving the Dirac equation from the Klein-Gordon equation; see, e.g., Ref. [20]. However, it does not mean that we cannot go beyond Dirac's minimal representation. As far as the dimensionality of the spinor degree of freedom is a multiple of four in the spatial three-dimensional case as in Eq. (15) below, it is possible to construct Dirac-type equations with additional internal degrees of freedom, which

*manami@iis.u-tokyo.ac.jp
†hatano@iis.u-tokyo.ac.jp
‡imura@iis.u-tokyo.ac.jp
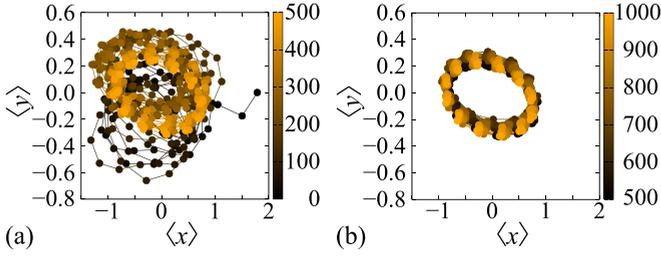§hideaki.obuse@eng.hokudai.ac.jp

FIG. 1. The expectation values $\langle x \rangle$ and $\langle y \rangle$ of the position of a 2D DTQW for (a) $0 \leqslant T \leqslant 500$ and for (b) $500 \leqslant T \leqslant 1000$. Black circles indicate the values at the beginning of time evolution; they turn into orange as time goes on. We set $\hbar = a = \Delta t = 1$.

is what we have done here. Thus we refer to our model as the extended Dirac Hamiltonian.

As another point, we might have had to refer to the square of the Dirac Hamiltonian as the Klein-Gordon equation, but we will below refer to it as the Schrödinger Hamiltonian because we will demonstrate the behavior of a harmonic oscillator under the linear spatial dependence of the mass terms $m_x(x)$ and $m_y(y)$. Indeed, the existence of the two mass terms in Eq. (1) is also a feature of our extended Dirac Hamiltonian.

The introduction of σ^x in Eq. (1) also enables corner states, the second-order topological states, to emerge. The higher-order topological states have come under intensive investigation lately (see, e.g., Refs. [17–19,21–26]). A systematic construction of Hamiltonians that harbors higher-order topological states was developed recently by Hayashi [22]. The extended Dirac Hamiltonian proposed in the present paper turns out to follow the construction of higher-order topological states, and hence the present two-dimensional DTQW explicitly exhibits corner states. In other words, the present DTQW models simulate quantum dynamics of higher-order topological insulators.

We numerically find that our 2D quantum walker behaves like a 2D harmonic oscillator, as shown in Fig. 1, to which we will get back below. We also reveal nontrivial topological properties of our DTQW using the implication of the Dirac Hamiltonian [27]. We also numerically find two different types of topological bound states, namely edge states of the topology of type $2\mathbb{Z}$ (which are robust against randomness in Fig. 2) and corner states, by manipulating the coin operators of our DTQW. (See below for the definitions of the notations in Figs. 1 and 2.)
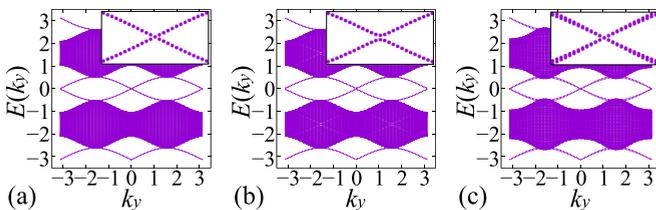

FIG. 2. Dispersion relation of the quasienergy spectra $E(k_y)$ with $\theta_1 = -\theta_2 = \pi/3$. (a) $\theta_y = 0$ and (b) $\theta_y = \pi/50$ without randomness, and (c) $\theta_y = 0$ with randomness $\Delta\theta_{x0}(x) \in [-0.25, 0.25]$. The central part of the dispersion is enlarged in the upper right corner in each panel. We set $\hbar = a = \Delta t = 1$.

A. Review of the one-dimensional case

Let us first review the continuum limit of the 1D DTQW. We define the time evolution of the standard 1D quantum walk $|\psi(T)\rangle = U^{(1)T}|\psi(0)\rangle$ for $T \in \mathbb{Z}$ in terms of the following coin and shift operators:

$$C := \sum_{x \in a\mathbb{Z}} |x\rangle\langle x| \otimes e^{-i\theta_x(x)\sigma^y}, \quad (2)$$

$$S := \sum_{x \in a\mathbb{Z}} (|x - a\rangle\langle x| \otimes |\mathrm{L}\rangle\langle\mathrm{L}| + |x + a\rangle\langle x| \otimes |\mathrm{R}\rangle\langle\mathrm{R}|) \quad (3)$$

with $U^{(1)} := SC$. Here, $\theta_x(x)$ is a coefficient set to a linear function of x below, a is the lattice constant, and $\{\sigma^x, \sigma^y, \sigma^z\}$ are the Pauli matrices in the space spanned by the leftward state, $|\mathrm{L}\rangle = (1, 0)^\top$, and the rightward state, $|\mathrm{R}\rangle = (0, 1)^\top$. We set $\hbar$ to unity throughout the paper.

Let us express the shift operator (3) in the form

$$S = \exp\left(-a\sigma^z \frac{d}{dx}\right) = \exp(-ia\sigma^z p_x) \quad (4)$$

with $p_x = -i\frac{d}{dx}$. Scaling the parameters a and $\theta_x(x)$ as in $\epsilon := a/\Delta t$ and $m_x(x) := \theta_x(x)/\Delta t$ with $t := T\Delta t$ and taking the limit $\Delta t \to 0$ with $T \to \infty$ under a fixed value of t, we find the continuum limit of the time-evolution operator in the form of the Trotter formula [13]

$$\lim_{\Delta t \to 0} U^{(1)T} = \lim_{\Delta t \to 0} [e^{-i\epsilon\Delta t\sigma^z p_x}e^{-im_x(x)\Delta t\sigma^y}]^T = e^{-iH_D^{(1)}t}, \quad (5)$$

where

$$H_D^{(1)} = \epsilon\sigma^z p_x + m_x(x)\sigma^y \quad (6)$$

represents the Hamiltonian of a Dirac particle with mass $m_x(x)$ in 1D. We can analyze its dynamics approximately by squaring it:

$$\left(H_D^{(1)}\right)^2 = (\epsilon^2 p_x{}^2 + m_x(x)^2)\sigma^0 - i\epsilon\sigma^x[p_x, m_x(x)] =: H_S^{(1)}, \quad (7)$$

where σ^0 denotes the 2×2 identity matrix for the space spanned by $|\mathrm{L}\rangle$ and $|\mathrm{R}\rangle$. Let us assume that $m_x(x) = \theta_x(x)/\Delta t$ is linear in x as in $\theta_x(x) = bx$ and $m_x(x) = \beta x$ with $\beta = b/\Delta t$. This reduces the last term of $H_S^{(1)}$ to $-\epsilon\beta\sigma^x$. A unitary transformation $V = \exp(i\sigma^y\pi/4)$ turns the last term further to $\epsilon\beta\sigma^z$, diagonalizing the Hamiltonian $H_S^{(1)}$ to the two blocks of

$$\tilde{H}_{S\pm}^{(1)} := \epsilon^2 p_x{}^2 + \beta^2 x^2 \pm \epsilon\beta, \quad (8)$$

each of which is the Schrödinger Hamiltonian in a 1D harmonic potential with a constant term under the following identification:

$$\epsilon^2 \leftrightarrow \frac{1}{2m_S}, \quad \beta^2 \leftrightarrow \frac{m_S\omega^2}{2}, \quad \epsilon\beta \leftrightarrow \frac{\omega}{2}. \quad (9)$$

The preceding argument shows that the Dirac and Schrödinger Hamiltonians share the same eigenvectors. Indeed, the time evolution of $H_D^{(1)}$ is approximately given by $\tilde{H}_S^{(1)}$. We can numerically confirm that the Dirac Hamiltonian makes a wave packet oscillate around $x = 0$ approximately like a harmonic oscillator.

II. TWO-DIMENSIONAL MODEL

Our first point of the paper is to extend the argument to higher dimensions. There have been two major kinds of 2D DTQW: the Grover walk [28] and an alternative quantum walk [14]. However, we cannot map either of them to the Schrödinger equation. Instead of these two DTQWs, we here introduce a DTQW whose continuum limit yields the extended Dirac Hamiltonian (1). Let $|L\rangle$, $|R\rangle$, $|D\rangle$, and $|U\rangle$ denote the basis vectors for the leftward, rightward, downward, and upward states, respectively. In Eq. (1), $\{\sigma^x, \sigma^y, \sigma^z\}$ are the the Pauli matrices for the space spanned by $|L\rangle$ and $|R\rangle$, while $\{\tau^x, \tau^y, \tau^z\}$ and τ^0 are the Pauli matrices and the identity matrix for the space spanned by $|D\rangle$ and $|U\rangle$. We let $m_x(x)$ and $m_y(y)$ denote the mass terms. The momenta p_x and p_y can be rewritten in the forms of $-i\partial/\partial x$ and $-i\partial/\partial y$, respectively.

We can easily confirm that the extended Dirac Hamiltonian (1) is, by squaring it, mapped to the Schrödinger Hamiltonian

$$H_S^{(2)} := H_{S_x} \otimes \tau^0 + \sigma^0 \otimes H_{S_y}, \qquad (10)$$

where

$$H_{S_x} := (\epsilon^2 p_x{}^2 + m_x(x)^2)\sigma_0 - i\epsilon\sigma^x[p_x, m_x(x)], \qquad (11)$$

$$H_{S_y} := (\epsilon^2 p_y{}^2 + m_y(y)^2)\tau^0 - i\epsilon\tau^x[p_y, m_y(y)]. \qquad (12)$$

Assumptions

$$m_x(x) = \beta x \quad \text{and} \quad m_y(y) = \beta y \qquad (13)$$

reduce Eq. (10) to

$$\begin{aligned}H_S^{(2)} := {}&(\epsilon^2 p_x{}^2 + \beta^2 x^2 - \epsilon\beta\sigma^x) \otimes \tau^0 \\ &+ \sigma^0 \otimes (\epsilon^2 p_y{}^2 + \beta^2 y^2 - \epsilon\beta\tau^x), \qquad (14)\end{aligned}$$

which represents a 2D harmonic oscillator under the identification (9).

We can further extend the argument into the 3D model with the extended Dirac Hamiltonian

$$H_D^{(3)} := H_{D_x} \otimes \tau^0 \otimes v^0 + \sigma^x \otimes H_{D_y} \otimes v^0 + \sigma^x \otimes \tau^x \otimes H_{D_z} \qquad (15)$$

although it may not be a standard 3D Dirac Hamiltonian because we have now $2 \times 2 \times 2$ degrees of freedom at each site. In Eq. (15), v^0 is the identity matrix for the space spanned by the backward state $|B\rangle$ and the forward state $|F\rangle$ of the additional inner degree of freedom, while $\{v^x, v^y, v^z\}$ are the Pauli matrices for the same space. Extension to even higher dimensions should be obvious.

A. Two-dimensional oscillator

We next construct our DTQW model from the extended Dirac Hamiltonian (1). The Hilbert space for the inner degrees of freedom at each site is now spanned by

$$(|L\rangle + |R\rangle) \oplus (|D\rangle + |U\rangle) = |LD\rangle + |RD\rangle + |LU\rangle + |RU\rangle. \qquad (16)$$

We hereafter fix the ordering of the basis vectors in this way. After conducting the Trotter decomposition on $\exp(-iH_D^{(2)}t)$,

we obtain the time-evolution operator $U^{(2)}$ in the form of $U^{(2)} = S_y C_y S_x C_x$ with

$$C_x := e^{-i\theta_x(x)(\sigma^y\otimes\tau^0)}, \qquad S_x := e^{-a(\sigma^z\otimes\tau^0)\partial_x},$$

$$C_y := e^{-i\theta_y(y)(\sigma^x\otimes\tau^y)}, \qquad S_y := e^{-a(\sigma^x\otimes\tau^z)\partial_y}. \qquad (17)$$

Let us here assume that $\theta_x(x)$ and $\theta_y(y)$ are linear in x and y, respectively, as in

$$\theta_x(x) = bx \quad \text{and} \quad \theta_y(y) = by, \qquad (18)$$

which are related to Eq. (13) as in $\theta_x(x) = m_x(x)\Delta t$ and $\theta_y(y) = m_y(y)\Delta t$. We can regard this as effective linear potentials for the corresponding Dirac particle. The operators C_x and S_x in the x direction are given by straightforwardly extending the corresponding operators (2) and (3) for the 1D DTQW, respectively. On the other hand, the operators C_y and S_y read

$$C_y = \begin{pmatrix} +c & & & -s \\ & +c & -s & \\ & +s & +c & \\ +s & & & +c \end{pmatrix},$$

$$S_y = \begin{pmatrix} P & Q & & \\ Q & P & & \\ & & P & -Q \\ & & -Q & P \end{pmatrix}, \qquad (19)$$

where

$$c := \cos(by), \quad s := \sin(by),$$

$$P := \tfrac{1}{2}(|y-a\rangle\langle y| + |y+a\rangle\langle y|),$$

$$Q := \tfrac{1}{2}(|y-a\rangle\langle y| - |y+a\rangle\langle y|). \qquad (20)$$

These coin and shift operators in Eq. (19) look different from the Grover walk [28] and the alternative quantum walk [14] because of the σ^x term in the extended Dirac Hamiltonian (1). We believe our DTQW to be better in representing 2D physics in the sense that it exhibits dynamics of a 2D harmonic oscillator, as we demonstrated in Fig. 1.

In the numerical calculation for Fig. 1, we set the system size to $L_x = L_y = 101$ with $-50 \leqslant x \leqslant 50$ and $-50 \leqslant y \leqslant 50$ under periodic boundary conditions in both directions. We used the effective potential of the form

$$\theta_{x_\mu}(x_\mu) = \begin{cases} \pi/4 & \text{for } 5 < x_\mu \leqslant 50, \\ bx_\mu & \text{for } |x_\mu| \leqslant 5, \\ -\pi/4 & \text{for } -50 \leqslant x_\mu < -5, \end{cases} \qquad (21)$$

where $x_1 = x$, $x_2 = y$, and $b = \pi/20$. We repeated numerical multiplication of $U^{(2)}$ to the initial state. For the initial state, we used an eigenstate of the eigenvalue unity of the time-evolution operator $U^{(2)}$ shifted in the x direction by two sites and imposed the initial velocity in the form of $e^{i(k_x x + k_y y)}$ with $(k_x, k_y) = (0, \pi)$. The eigenstate of the eigenvalue unity of $U^{(2)}$ is in the Trotter limit given by the Gaussian form of the zero-energy eigenvalue of our extended 2D Dirac Hamiltonian (1), which we explicitly obtain in Appendix A 2 b.

Figure 1 shows the expectation values,

$$\langle x(T)\rangle := \sum_{x,y} x P(x, y, T),$$

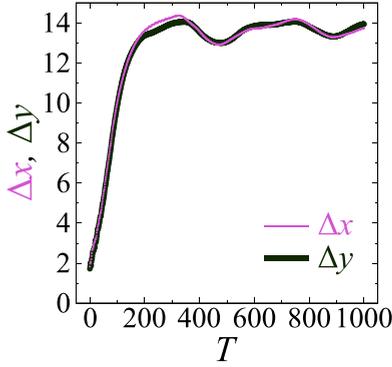$$\langle y(T)\rangle := \sum_{x,y} y P(x, y, T), \qquad (22)$$

FIG. 3. The time-step dependence of the standard deviations Δx (thin purple line) and Δy (thick dark green line) of the quantum walker in 2D. We set $\hbar = a = \Delta t = 1$.

at each time step, where $P(x, y, T)$ is the quantum probability at site (x, y) at time step T and satisfies $\sum_{x,y} P(x, y, T) = 1$. We observe the circular trajectory in Fig. 1; after some time it converges to an orbit of a limit cycle [Fig. 1(b)], which closely resembles the one of a Schrödinger dynamics under a 2D harmonic potential. In Fig. 3, we can see that the standard deviations almost converge to a constant after $T \sim 500$, which implies that the walker reaches a steady state of a circling wave packet around the time. With these facts, we believe that we successfully observe dynamics that resembles the 2D harmonic oscillator. We confirm in Appendix A 2 b that all the eigenstates of the corresponding 2D extended Dirac Hamiltonian (1) are composed of the eigenstates of a 2D harmonic oscillator.

The fact that the present 2D DTQW behaves like a 2D harmonic oscillator is particularly important to some of the present authors for studies of quantum active matter. They defined in Ref. [29] a quantum version of the active Brownian particle [30], in which Schweitzer *et al.* numerically demonstrated that a classical active particle climbs up the 2D harmonic potential and makes a circular orbit. Some of the present authors [29] are reproducing similar movement of the quantum version, using the present oscillator behavior of the 2D DTQW. This is why the present quantum walker making the circular orbit is critically important.

B. Topological edge states of two-dimensional DTQW

Let us turn to topological properties of DTQW. Jackiw and Rebbi [27] suggested that when a Dirac system, e.g., Eq. (6) (presumed to be extended to infinity), has two domains in each of which the mass term takes a different value, e.g.,

$$m_x(x) = \begin{cases} m_1 & \text{for } x > 0, \\ m_2 & \text{for } x < 0, \end{cases} \tag{23}$$

then a robust zero-energy state spatially localized in the vicinity of the domain wall emerges in the mass gap iff the signs of m_1 and m_2 differ [31]. In other words, the zero-energy domain-wall state is protected by an index ν_1 defined as $(-1)^{\nu_1} = \text{sgn}(m_1)\text{sgn}(m_2)$, which takes two integral values $\nu_1 = 0, 1$ in this particular case. Now that the concept of a topological insulator is well established, Jackiw and Rebbi's example is recognized as its earliest realization, and the index

ν_1 is interpreted as a topological number. Indeed, the model (6) belongs to the symmetry class DIII with the topology of type $\mathbb{Z}_2$ in 1D [32,33].

We checked it numerically using the 1D DTQW prescribed by Eqs. (2) and (3) with $\theta_x(x)$ having two domains,

$$\theta_x(x) = \begin{cases} \theta_1 & \text{for } |x| < L_1, \\ \theta_2 & \text{for } L_1 < |x| < [L_x/2]. \end{cases} \tag{24}$$

Note that each of the domain walls at $x = \pm L_1$ corresponds to the one in Eq. (23) as in $\theta_x(x) = m_x(x)\Delta t$. Since our DTQW is under the periodic boundary condition, there are two domain walls with discontinuities in $m_x(x)$ at $x = \pm L_1$, and therefore we observed two topologically protected zero-energy states, each of which is localized at a different domain wall. [Incidentally, squaring the Dirac Hamiltonian as in Eq. (7), we find that the last term of $H_S^{(1)}$ yields delta functions at the discontinuities of $m_x(x)$, and thus the edge states of the Dirac Hamiltonian can also be interpreted as bound states of the corresponding Schrödinger particle to the delta potentials.]

In the 2D realization of our DTQW prescribed by Eqs. (17) and (19), using again the domain-wall configuration of $\theta_x(x)$ introduced in the 1D case with $\theta_y(y) \equiv 0$ in Eq. (17), the protected zero-energy states acquire a dispersion; see Appendix A 3 b for the solution in the case of the 2D extended Dirac Hamiltonian (1). Figure 2(a) shows quasienergy spectrum $E_n = -i \ln U_n^{(2)}$ for each $k_{y_n} = 2n\pi/L_y$ with $\theta_y = 0$. We observe that two linear dispersions with positive and negative slopes completely traverse the bulk energy gap, manifesting the feature of protected gapless edge states. Their gaplessness is protected by a topological number $\nu_1 = 1$ introduced above; when ν_1 changes upon changing $\theta_x(x)$, the bulk energy gap must close once and reopen in the space of control parameters, where different topological phases are defined.

The extended Dirac Hamiltonian (1) with $m_y = 0$ has a time-reversal symmetry under $\Theta = \sigma^x \otimes \tau^y K$ with K being complex conjugation, a particle-hole symmetry under $\Xi = \mathbb{I}_{4\times4} K$, and a chiral symmetry under $\Pi = \sigma^x \otimes \tau^y$, and hence belongs to the symmetry class DIII with a topology of type $\mathbb{Z}_2$ in 2D [32,33]. However, the time-evolution operator $U^{(2)} = S_y S_x C_x$ (with $\theta_y = 0$) only has the particle-hole symmetry under $\Xi = \mathbb{I}_{4\times4} K$ because of the specific ordering of $S_y S_x$ ($\neq S_x S_y$), and hence our DTQW belongs to the symmetry class D with a topology of type $\mathbb{Z}$ in 2D [32,33]. (Incidentally, we have an additional sublattice symmetry in S_y. Adding the phase $e^{i\pi}$ to the every other y and shifting k_y with π do not change S_y. This results in a π periodicity in k_y in the spectra in Fig. 2.)

We can understand the structure of the dispersion of edge states in Fig. 2(a) as in Fig. 4. Let us first note that our time-evolution operator $U^{(2)} = S_y S_x C_x$ for $\theta_y = 0$ is block diagonalized for the blocks $\tau^z = \pm 1$ with the same absolute value of k_y but with a different sign. Since each block belongs to the class D, we have a topology of type $2\mathbb{Z}$. In the block of $\tau^z = 1$, namely $|D\rangle$, an edge state localized at $x = -L_1 = -25$ in Fig. 5 has the dispersion of a positive slope and one at $x = L_1 = 25$ has one with a negative slope as shown in Fig. 4. In the block of $\tau^z = -1$, namely $|U\rangle$, on the other hand, an edge state at $x = -L_1 = -25$ has the dispersion with a negative slope and the other at $x = L_1$ has one with a positive slope. Since the two blocks have opposite signs of k_y, the
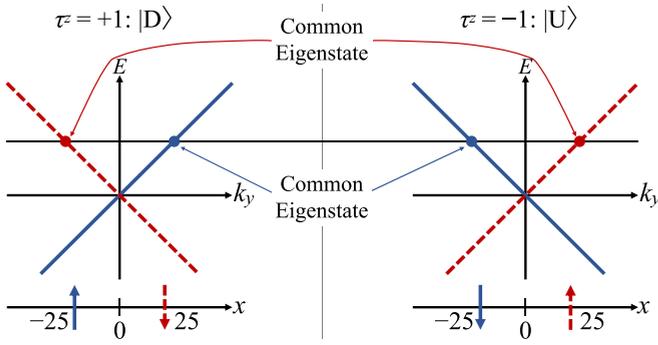
FIG. 4. Schematic representation of the dispersion around $k_y = 0$ in Fig. 2(a). We set $\hbar = a = \Delta t = 1$.

dispersion has a mirror symmetry, and hence the eigenstates on the two solid lines in Fig. 4 are common to each other; the same applies to the eigenstates on the broken lines. This is why we observe the lines with both positive and negative slope crossing at $k_y = 0$. Two eigenvalues are degenerate on each line.

Upon introducing a nonzero value of θ_y, which is incompatible with the dictated symmetry of class D, a gap emerges around $k_y = 0$ as shown in Fig. 2(b). Meanwhile, the topological edge states are robust against other types of small perturbation, which we numerically confirm by introducing randomness. We added to $\theta_x(x)$ a random perturbation $\Delta\theta_{x0}(x)$, randomly choosing independently for each site uniformly from the range $[-0.25, 0.25]$. As we see in Fig. 2(c), the degeneracy for $\tau^z = \pm 1$ is lifted but the crossing at $k_y = 0$ remains.

C. Chiral symmetry and higher-order topology

In Fig. 2(b) and in its description, we saw that the presence of a finite value of θ_y is incompatible with the symmetry dictated in the periodic table for the symmetry class D, and hence the edge states protected by the standard first-order topology have been gapped out. However, we now see that the chiral symmetry inherent to the 1D Dirac Hamiltonian (6) leads to the emergence of the so-called higher-order topology [21–26], which is beyond the standard classification of topological insulators dictated by the periodic table given in Refs. [32,33].
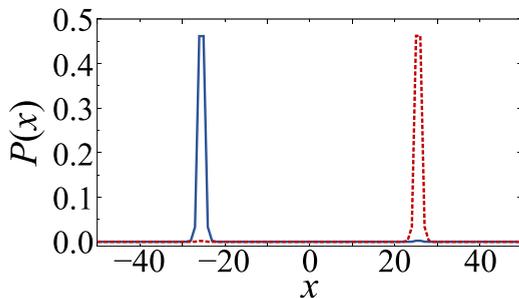

FIG. 5. Probability density of an edge state localized around $x = -25$ (solid blue line) and one localized around $x = 25$ (red broken line) with $k_y = 0$ and the zero quasienergy in the spectrum of Fig. 2(a). We set $\hbar = a = \Delta t = 1$.

The standard topological insulator is characterized by the existence of protected gapless or zero-energy surface states. In d space dimensions, such surface states appear on $(d-1)$-dimensional surfaces of the system. In the case of the recently proposed higher-order topological insulator [21–26], not only the d-dimensional bulk but also the $(d-1)$-dimensional surfaces are both gapped, and yet some higher-order, e.g., $(d-n)$-dimensional "surfaces" (an extremity of the system with co-dimension n), remain gapless with $n \geqslant 2$. To represent such a higher-order surface, the word "corner" is most commonly employed, which in the case of $d = 2$ and $n = 2$ as in the present case is consistent with the common usage of the word, as we will see below.

Let us note that the Pauli matrix σ^x introduced along with H_{D_y} in Eq. (1) is nothing but the chiral operator, i.e., $\Gamma_1 = \sigma^x$, associated with the 1D Dirac Hamiltonian H_{D_x}:

$$\{\Gamma_1, H_{D_x}\} = 0 \quad \text{with} \quad \Gamma_1^2 = 1. \tag{25}$$

This being said, we notice that the construction of the 2D extended Dirac Hamiltonian in Eq. (1) is done precisely in the same manner as in the recipe in Ref. [22] for constructing the second- and higher-order (nth-order) topological insulators, starting with the standard first-order topological insulators H_1 and H_2 as its building blocks, where H_1 must have the chiral symmetry Γ_1 as in $\{\Gamma_1, H_1\} = 0$ with $\Gamma_1^2 = 1$. One can indeed show that the Hamiltonian $H^{(2)}$ constructed as

$$H^{(2)} = H_1 \otimes 1 + \Gamma_1 \otimes H_2 \tag{26}$$

has the designed property of the second-order topological insulator [22]. Higher-order (nth-order) topological insulators $H^{(n)}$ are constructed with $n-1$ chiral operators and n Hamiltonian of which at least $n-1$ anticommute with the corresponding chiral operators:

$$H^{(n)} = \underbrace{H_1 \otimes 1 \otimes 1 \otimes \cdots \otimes 1 \otimes 1}_{n} + \underbrace{\Gamma_1 \otimes H_2 \otimes 1 \otimes \cdots \otimes 1 \otimes 1}_{n}$$
$$+ \cdots + \underbrace{\Gamma_1 \otimes \Gamma_2 \otimes \Gamma_3 \otimes \cdots \otimes \Gamma_{n-1} \otimes H_n}_{n} \tag{27}$$

with

$$\{\Gamma_i, H_i\} = 0, \quad \Gamma_i^2 = 1, \quad i = 1, \ldots, n-1. \tag{28}$$

In the present case of our 2D extended Dirac Hamiltonian (1), we can naturally identify the constituents as $H_1 = H_{D_x}$ and $H_2 = H_{D_y}$. Appendix A 3 c shows that the zero-energy eigenstate of our 2D extended Dirac Hamiltonian is the product of the zero-energy edge state running in the y direction and that running in the x direction, which results in the corner states demonstrated below in Fig. 6 for our 2D DTQW model. Surprisingly, our 3D extended Dirac Hamiltonian (15) naturally satisfies the conditions (27) and (28) under the identification of $H_1 = H_{D_x}$, $H_2 = H_{D_y}$, and $H_3 = H_{D_z}$. We can naturally apply the same argument to the 3D case as in the 2D case.

The appearance or nonappearance of a higher-order topological state (specifically a zero-energy corner state in the case of $n = 2$) is encoded in a topological index $\nu^{(n)}$ expressed (at least for a corner with a right angle [24,34]) as a product of
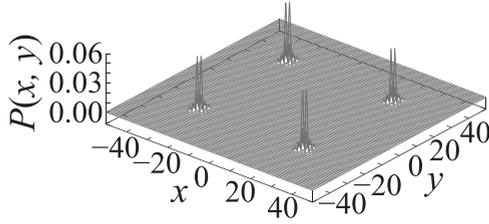
FIG. 6. Probability distribution of zero-energy corner states with the potential $\theta_x(x)$ and $\theta_y(y)$ specified in the main text. We here plot one out of the totally eight corner states that are degenerate to a nearly zero eigenvalue. We set $\hbar = a = \Delta t = 1$.

conventional topological indices

$$\nu^{(n)} = \prod_{m=1}^{n} \nu_m, \tag{29}$$

where each ν_m provides information on the existence and the absence of a gapless $(d-1)$-dimensional surface state of the constituent first-order topological insulators H_m in d dimensions.

Specifically for $n = 2$ and $d = 2$ in the present case, as each of the two indices ν_1 and ν_2 encodes information on the existence and the absence of a gapless one-dimensional surface state, the situation $\nu_1, \nu_2 = 0$ corresponds to the absence, indicating that the system is trivial, while the situation $\nu_1, \nu_2 \neq 0$ signifies that the system is topologically nontrivial, so that $\nu^{(2)}$ encodes information on the existence and absence of a gapless zero-dimensional corner state.

In order to let corner states emerge in our 2D DTQW model, we introduce the domain structure in the x direction also in the y direction; we set $\theta_y(y)$ such that

$$\theta_y(y) = \begin{cases} \theta_1 & \text{for } |y| < L_2, \\ \theta_2 & \text{for } L_2 < |y| < [L_y/2] \end{cases} \tag{30}$$

in addition to the one in Eq. (24). We chose the parameter values specifically as $\theta_1 = -\theta_2 = \pi/3$, $L_x = L_y = 101$, and $L_1 = L_2 = 25$ for numerical calculation for Fig. 6. We can observe four zero-energy corner states localized at the four corners of the domain $|x| < L_1$ with $|y| < L_2$. Note that each corner state is defined as localized at one of the four corners of the domain; the state represented in Fig. 6 is a superposition of the four corner states.

III. SUMMARY

To summarize, we proposed a DTQW in multidimensional systems, whose continuum limit is the extended Dirac equation which can be further mapped to the Schrödinger equation. We successfully reproduced with our DTQW the dynamics similar to that of a Schrödinger particle under a harmonic potential. We also observed topological edge and corner states with discontinuous effective potentials in one- and two-dimensional systems simply by manipulating the coin operators of our DTQW. We thereby claim that the present DTQW is a powerful platform of numerical simulation and experimental implementation of the Dirac and Schrödinger particles.
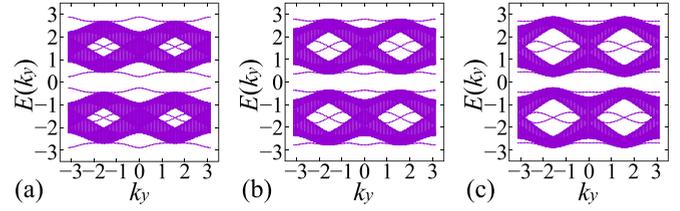

FIG. 7. Dispersion relation of the quasienergy spectra $E(k_y)$ for the domain-wall structure in $\theta_x(x)$ as specified in the main text with (a) $\theta_y = \pi/6$, (b) $\theta_y = \pi/4$, and (c) $\theta_y = \pi/3$. We set $\hbar = a = \Delta t = 1$.

As a final remark, increasing θ_y further from the case in Fig. 2(b), we find the spectrum in Fig. 7. We have numerically confirmed that the states enclosed in the openings of the bulk bands are edge states; see Appendix B of the bulk band structure. This implies that our DTQW accommodates a further symmetry that protects these enclosed edge states, but we have not resolved yet what symmetry it is.

APPENDIX A: EIGENVALUES OF THE 2D EXTENDED DIRAC HAMILTONIAN

In the present Appendix, we describe how to obtain the eigenvalues and eigenvectors of our 2D extended Dirac Hamiltonian (1) out of those of the 1D Dirac Hamiltonian (6). The former should give the quasienergy eigenvalues and eigenvectors of our 2D DTQW within the Trotter approximation, particularly near zero energy, that is, near the eigenvalue unity of the time-evolution operator.

We first introduce the general formalism in Appendix A 1. We then present the explicit solutions in the case of linear mass terms in Appendix A 2 and in the case of stepwise mass terms in Appendix A 3.

1. General formalism

We first set the eigenstates of H_{D_x} H_{D_y} as in

$$H_{D_x}|\psi_{E_x}^{D,(1)}\rangle = E_x|\psi_{E_x}^{D,(1)}\rangle, \tag{A1}$$

$$H_{D_y}|\psi_{E_y}^{D,(1)}\rangle = E_y|\psi_{E_y}^{D,(1)}\rangle \tag{A2}$$

with the normalization

$$\langle\psi_{E_x}^{D,(1)}|\psi_{E_x}^{D,(1)}\rangle = \langle\psi_{E_y}^{D,(1)}|\psi_{E_y}^{D,(1)}\rangle = 1. \tag{A3}$$

As shorthand, let their direct product be denoted by

$$|\psi_{E_x,E_y}^{D,(1)}\rangle := |\psi_{E_x}^{D,(1)}\rangle|\psi_{E_y}^{D,(1)}\rangle. \tag{A4}$$

We now assume the ansatz for the eigenstate of our 2D extended Dirac Hamiltonian

$$H_D^{(2)} := H_{D_x} \otimes \tau^0 + \sigma^x \otimes H_{D_y} \tag{A5}$$

of the form

$$\left|\psi_E^{D,(2)}\right\rangle = (\gamma + \delta\sigma^x)\left|\psi_{E_x,E_y}^{D,(1)}\right\rangle, \qquad (A6)$$

where γ and δ are real coefficients to be determined hereafter. From the eigenvalue equation

$$H_D^{(2)}\left|\psi_E^{D,(2)}\right\rangle = E\left|\psi_E^{D,(2)}\right\rangle, \qquad (A7)$$

we obtain

$$[\gamma(E_x + E_y\sigma^x) + \delta(-E_x\sigma^x + E_y)]\left|\psi_{E_x,E_y}^{D,(1)}\right\rangle$$
$$= E(\gamma + \delta\sigma^x)\left|\psi_{E_x,E_y}^{D,(1)}\right\rangle, \qquad (A8)$$

where we used the anticommutation relation

$$\{H_{D_x}, \sigma^x\} = \{(\epsilon\sigma^z p_x + m_x(x)\sigma^y), \sigma^x\} = 0. \qquad (A9)$$

We thereby find the equations for the coefficients as

$$\gamma E_x + \delta E_y = \gamma E, \qquad (A10)$$

$$\gamma E_y - \delta E_x = \delta E. \qquad (A11)$$

First, let us eliminate E from the set of the equations. We then find

$$2\gamma\delta E_x = (\gamma^2 - \delta^2)E_y, \qquad (A12)$$

which motivates us to define the transformations of the coefficients of the forms

$$\gamma = A\cos\phi, \quad \delta = A\sin\phi. \qquad (A13)$$

We then have from Eq. (A12)

$$\tan 2\phi = \frac{E_y}{E_x}, \qquad (A14)$$

which determines the phase coefficient ϕ for the specific solutions of Eqs. (A1) and (A2). The amplitude coefficient A, on the other hand, is found from the normalization

$$1 = \left\langle\psi_E^{D,(2)}\middle|\psi_E^{D,(2)}\right\rangle = \gamma^2 + \delta^2 + 2\gamma\delta s$$
$$= A^2(1 + s\sin 2\phi), \qquad (A15)$$

where $s := \left\langle\psi_{E_x}^{D,(1)}\middle|\sigma^x\middle|\psi_{E_x}^{D,(1)}\right\rangle$. We let A be undetermined in the present Appendix since it depends on the specific form of the eigenstate $\left|\psi_{E_x}^{D,(1)}\right\rangle$.

The set of equations (A10) and (A11) further produces

$$E_x = E\cos 2\phi, \quad E_y = E\sin 2\phi, \qquad (A16)$$

and hence

$$E = \pm\sqrt{E_x^2 + E_y^2}. \qquad (A17)$$

This implies that our 2D extended Dirac Hamiltonian (1) is indeed a precise direct product of independent components of 1D Dirac Hamiltonians H_{D_x} and H_{D_y}, and further implies that the 2D DTQW presented in Sec. II is also a precise direct product of independent components of 1D DTQW in the x and y directions

From Eq. (A17) we can conclude the following. First, the zero-energy eigenstate of $H_D^{(2)}$, if any, can be constructed only from the zero-energy eigenstates of H_{D_x} and H_{D_y}, which is indeed simply given by

$$\left|\psi_{E=0}^{D,(2)}\right\rangle = \left|\psi_{E_x=0}^{D,(1)}\right\rangle\left|\psi_{E_y=0}^{D,(1)}\right\rangle. \qquad (A18)$$

Second, if there is an energy gap in the spectrum of either of H_{D_x} or H_{D_y}, then the spectrum of $H_D^{(2)}$ has an energy gap.

2. Case of the linear potentials (13)

We here explicitly obtain the Gaussian form of the zero-energy eigenstate of the 2D extended Dirac Hamiltonian (1) under the linear potentials (13). The eigenstate of the eigenvalue unity of the time-evolution operator $U(2)$, which is the state that we used for the initial state of our simulation in Sec. II A, is given by the state given here within the Trotter approximation.

a. Eigenvalues of the 1D Dirac Hamiltonian (6)

Let us first derive eigenstates of the 1D Dirac Hamiltonian (6) with $m_x(x) = \beta x$. The Schrödinger Hamiltonian after the unitary transformation $V = \exp(i\sigma^y\pi/4)$ reads

$$\tilde{H}_S^{(1)} := \begin{pmatrix} \tilde{H}_{S_+}^{(1)} & 0 \\ 0 & \tilde{H}_{S_-}^{(1)} \end{pmatrix}, \qquad (A19)$$

where $\tilde{H}_{S_\pm}^{(1)} := \epsilon^2 p_x^2 + \beta^2 x^2 \pm \epsilon\beta$ as in Eq. (8). Each of the block Hamiltonians can be rewritten in the form

$$\tilde{H}_{S_\pm}^{(1)} = \omega\left(\hat{a}^\dagger\hat{a} + \frac{1}{2} \pm \frac{1}{2}\right) \qquad (A20)$$

with the ladder operators

$$\hat{a}^\dagger = \frac{1}{\sqrt{2}}\left(-\sqrt{\frac{\epsilon}{\beta}}\frac{d}{dx} + \sqrt{\frac{\beta}{\epsilon}}x\right),$$
$$\hat{a} = \frac{1}{\sqrt{2}}\left(\sqrt{\frac{\epsilon}{\beta}}\frac{d}{dx} + \sqrt{\frac{\beta}{\epsilon}}x\right), \qquad (A21)$$

where we employed the same identification for ϵ, β, and ω as in Eq. (9). Therefore, the Hamiltonian (A19) is rewritten as follows:

$$\tilde{H}_S^{(1)} = \omega\left(\hat{a}^\dagger\hat{a} + \frac{1}{2} + \frac{1}{2}\sigma^z\right) = \omega\begin{pmatrix} \hat{a}^\dagger\hat{a} + 1 & 0 \\ 0 & \hat{a}^\dagger\hat{a} \end{pmatrix}. \quad (A22)$$

We thus find for the Hamiltonian (A22) that the following two eigenstates are degenerate in the energy eigenvalue $n\omega$ with $n > 0$:

$$\left|\tilde{\psi}_{E_{x1}}^{S,(1)}\right\rangle = \begin{pmatrix} |n-1\rangle \\ 0 \end{pmatrix} \quad \text{and} \quad \left|\tilde{\psi}_{E_{x2}}^{S,(1)}\right\rangle = \begin{pmatrix} 0 \\ |n\rangle \end{pmatrix}. \quad (A23)$$

On the other hand, the eigenstate of the zero-energy eigenvalue is uniquely given by

$$\left|\tilde{\psi}_{E_x=0}^{S,(1)}\right\rangle = \begin{pmatrix} 0 \\ |0\rangle \end{pmatrix}. \qquad (A24)$$

We then obtain the eigenstates of energy eigenvalue $n\omega$ (with $n > 0$) of the Hamiltonian $H_S^{(1)}$ defined in Eq. (7) by a unitary transformation $V^\dagger = \exp(-i\sigma^y\pi/4)$ as arbitrary superpositions of the following two states:

$$\left|\psi_{E_{x1}}^{S,(1)}\right\rangle = \frac{1}{\sqrt{2}}\begin{pmatrix} |n-1\rangle \\ |n-1\rangle \end{pmatrix} \quad \text{and} \quad \left|\psi_{E_{x2}}^{S,(1)}\right\rangle = \frac{1}{\sqrt{2}}\begin{pmatrix} -|n\rangle \\ |n\rangle \end{pmatrix}. \quad (A25)$$

The unitary transformation above, upon being applied to Eq. (A24), gives the eigenstate of the zero-energy eigenvalue

of the Hamiltonian (7) as follows:

$$|\psi_{E_x=0}^{\mathrm{S},(1)}\rangle = \frac{1}{\sqrt{2}}\begin{pmatrix} -|0\rangle \\ |0\rangle \end{pmatrix}. \tag{A26}$$

More specifically, the eigenfunction of the zero-energy eigenvalue takes the Gaussian form

$$\psi_0^{(1)}(x) := \langle x|\psi_{E_x=0}^{\mathrm{S},(1)}\rangle = \left(\frac{\beta}{4\pi\epsilon}\right)^{1/4}\begin{pmatrix} -1 \\ 1 \end{pmatrix}\exp\left[-\frac{\beta}{2\epsilon}x^2\right]. \tag{A27}$$

Since the Schrödinger Hamiltonian $H_{\mathrm{S}}^{(1)}$ in Eq. (7) is the square of the 1D Dirac Hamiltonian (6), we anticipate that the two degenerate eigenstates in the eigenvalue $n\omega$ of the former Hamiltonian split into the eigenstates of the eigenvalues $\pm\sqrt{n\omega}$ of the latter Hamiltonian. In fact, by superposing the two states in Eq. (A25), we obtain a unique eigenstate of each of the energy eigenvalues $\sqrt{n\omega}$ and $-\sqrt{n\omega}$. Since the eigenstates are superpositions of the two states in Eq. (A25), we first write the eigenstates as

$$\frac{A}{\sqrt{2}}\begin{pmatrix} |n-1\rangle \\ |n-1\rangle \end{pmatrix} + \frac{B}{\sqrt{2}}\begin{pmatrix} -|n\rangle \\ |n\rangle \end{pmatrix} \tag{A28}$$

and determine the relationship between the coefficients A and B.

Let us operate the 1D Dirac Hamiltonian (6) from the left to the state above. We can utilize the following expressions of x and p_x in terms of the ladder operators in Eq. (A21):

$$x = \frac{1}{\sqrt{2}}\sqrt{\frac{\epsilon}{\beta}}(\hat{a}^\dagger + \hat{a}), \quad p_x = i\frac{1}{\sqrt{2}}\sqrt{\frac{\beta}{\epsilon}}(\hat{a}^\dagger - \hat{a}). \tag{A29}$$

These expressions let us rewrite the 1D Dirac Hamiltonian (6) with its mass being $m_x(x) = \beta x$ as follows:

$$\begin{aligned} H_{\mathrm{D}}^{(1)} &= \epsilon\sigma^z p_x + \beta x\sigma^y \\ &= \begin{pmatrix} \epsilon p_x & -i\beta x \\ i\beta x & -\epsilon p_x \end{pmatrix} \\ &= \frac{\sqrt{\omega}}{2}\begin{pmatrix} -i(\hat{a}^\dagger - \hat{a}) & -i(\hat{a}^\dagger + \hat{a}) \\ i(\hat{a}^\dagger + \hat{a}) & i(\hat{a}^\dagger - \hat{a}) \end{pmatrix}. \end{aligned} \tag{A30}$$

Hence operating the 1D Dirac Hamiltonian (6) to the state (A28) from the left yields

$$\begin{aligned} &H_{\mathrm{D}}^{(1)}\left[\frac{A}{\sqrt{2}}\begin{pmatrix} |n-1\rangle \\ |n-1\rangle \end{pmatrix} + \frac{B}{\sqrt{2}}\begin{pmatrix} -|n\rangle \\ |n\rangle \end{pmatrix}\right] \\ &= \sqrt{n\omega}\left[-i\frac{B}{\sqrt{2}}\begin{pmatrix} |n-1\rangle \\ |n-1\rangle \end{pmatrix} + i\frac{A}{\sqrt{2}}\begin{pmatrix} -|n\rangle \\ |n\rangle \end{pmatrix}\right]. \end{aligned} \tag{A31}$$

We take $iA = \pm B$ and $\mp iB = A$ in order for the state (A28) to be the eigenstates of the eigenvalues $\pm\sqrt{n\omega}$.

Thus, the eigenstate of the eigenvalue $+\sqrt{n\omega}$ of the 1D Dirac Hamiltonian (6) is uniquely given in the form of

$$|\psi_{E_x=+\sqrt{n}}^{\mathrm{D},(1)}\rangle = \frac{1}{\sqrt{2}}\begin{pmatrix} |n-1\rangle \\ |n-1\rangle \end{pmatrix} + \frac{i}{\sqrt{2}}\begin{pmatrix} -|n\rangle \\ |n\rangle \end{pmatrix}, \tag{A32}$$

while the eigenstate of the eigenvalue $-\sqrt{n\omega}$ of the 1D Dirac Hamiltonian (6) is uniquely given in the form of

$$|\psi_{E_x=-\sqrt{n}}^{\mathrm{D},(1)}\rangle = \frac{1}{\sqrt{2}}\begin{pmatrix} |n-1\rangle \\ |n-1\rangle \end{pmatrix} - \frac{i}{\sqrt{2}}\begin{pmatrix} -|n\rangle \\ |n\rangle \end{pmatrix}. \tag{A33}$$

Meanwhile, we can easily confirm that the eigenstate of the zero-energy eigenvalue of the Schrödinger Hamiltonian (7) is also the eigenstate of the zero-energy eigenvalue of the Dirac Hamiltonian (6) by operating it to the state (A26):

$$|\psi_{E_x=0}^{\mathrm{D},(1)}\rangle = \frac{1}{\sqrt{2}}\begin{pmatrix} -|0\rangle \\ |0\rangle \end{pmatrix}. \tag{A34}$$

b. Eigenvalues of the 2D extended Dirac Hamiltonian (1)

We now construct the eigenstates of the 2D Dirac Hamiltonian (1) out of the eigenstates (A32)–(A34) of the 1D Dirac Hamiltonian (6) following the general formalism presented in Appendix A 1.

Let us first find the state of the zero eigenvalue. According to Eq. (A18) of the general formalism, the zero-energy eigenstate of the 2D Hamiltonian $H_{\mathrm{D}}^{(2)}$ is the direct product of the zero-energy eigenstates of the 1D Hamiltonians H_{D_x} and H_{D_y}:

$$|\psi_{E_x=0}^{\mathrm{D},(1)}\rangle|\psi_{E_y=0}^{\mathrm{D},(1)}\rangle = \frac{1}{2}\begin{pmatrix} -|0\rangle \\ |0\rangle \end{pmatrix}\otimes\begin{pmatrix} -|0\rangle \\ |0\rangle \end{pmatrix}. \tag{A35}$$

More specifically, the eigenfunction of the zero-energy eigenvalue takes the following 2D Gaussian form:

$$\begin{aligned} \psi_0^{(2)}(x, y) &= \langle x|\psi_{E_x=0}^{\mathrm{D},(1)}\rangle\langle y|\psi_{E_y=0}^{\mathrm{D},(1)}\rangle \\ &= \sqrt{\frac{\beta}{4\pi\epsilon}}\begin{pmatrix} -1 \\ 1 \end{pmatrix}\otimes\begin{pmatrix} -1 \\ 1 \end{pmatrix}\exp\left[-\frac{\beta}{2\epsilon}(x^2 + y^2)\right]. \end{aligned} \tag{A36}$$

This 2D Gaussian form is indeed close to what we used for the initial state in the numerical simulation of Fig. 1.

For nonzero eigenvalues, combinations of the 1D states with the eigenvalues $\pm\sqrt{m\omega}$ and with the eigenvalues $\pm\sqrt{n\omega}$ produce the 2D states with the eigenvalues $\pm\sqrt{(m+n)\omega}$ as in Eq. (A17). The eigenstates are given in the form (A6) with the coefficients specified by Eqs. (A13)–(A15), or more specifically by $\tan 2\phi = \pm\sqrt{n/m}$. The degeneracy of the eigenvalues is the same as in the case of the 2D harmonic oscillator.

3. Topological edge states and higher-order topological corner state

We finally show that our 2D extended Dirac Hamiltonian (1) with Eqs. (24) and (30) has a zero-energy eigenstate in the product form of the zero-energy eigenstates of the 1D Dirac Hamiltonians (6) in the x and y directions, each of which is under one of Eqs. (24) and (30), respectively. Since the zero-energy eigenstate of each of the latter Hamiltonians is an edge state, the zero-energy eigenstate of the former Hamiltonian is a corner state, being the product of edge states in different directions.

a. First-order topological edge state in 1D

We first solve the eigenvalue problem of the 1D Dirac Hamiltonian (6)

$$H_{\mathrm{D}}^{(1)}\big|\psi_{E_x}^{\mathrm{D},(1)}\big\rangle = (\epsilon\sigma^z p_x + m_x(x)\sigma^y)\big|\psi_{E_x}^{\mathrm{D},(1)}\big\rangle$$
$$= E_x\big|\psi_{E_x}^{\mathrm{D},(1)}\big\rangle, \tag{A37}$$

where the mass term has a domain wall of the form

$$m_x(x) = \begin{cases} +m_0 & \text{for } x > 0, \\ -m_0 & \text{for } x < 0. \end{cases} \tag{A38}$$

We show that there is a bound state with the zero-energy eigenstate and scattering states with continuum spectra but with an energy gap.

Let us first focus on the bound state, assuming the zero-energy eigenvalue for explanatory purposes; see Ref. [31] for a solution without the assumption. When we are focused on the zero-energy eigenvalue, the right-hand side of Eq. (A37) vanishes, and therefore

$$(\epsilon\sigma^z p_x + m_x(x)\sigma^y)\big|\psi_{E_x=0}^{\mathrm{D},(1)}\big\rangle = 0. \tag{A39}$$

For $x > 0$, we have $m_x(x) = +m_0$, and hence the two rows of Eq. (A39) respectively read

$$-i\epsilon\frac{d}{dx}\psi_1 - im_0\psi_2 = 0, \tag{A40}$$

$$i\epsilon\frac{d}{dx}\psi_2 + im_0\psi_1 = 0, \tag{A41}$$

where we used the notation

$$\langle x|\psi_{E_x=0}^{\mathrm{D},(1)}\rangle = \begin{pmatrix} \psi_1(x) \\ \psi_2(x) \end{pmatrix}. \tag{A42}$$

Since we obtain

$$\frac{d^2}{dx^2}\psi_1 = \frac{m_0}{\epsilon}\frac{d}{dx}\psi_2 = \left(\frac{m_0}{\epsilon}\right)^2\psi_1, \tag{A43}$$

the convergent solution for $x > 0$ is found to be $\psi_1 \propto \psi_2 \propto e^{-(m_0/\epsilon)x}$. For $x < 0$, instead of Eq. (A43), we have

$$\frac{d^2}{dx^2}\psi_1 = -\frac{m_0}{\epsilon}\frac{d}{dx}\psi_2 = \left(\frac{m_0}{\epsilon}\right)^2\psi_1, \tag{A44}$$

and hence the convergent solution for $x < 0$ is given by $\psi_1 \propto \psi_2 \propto e^{+(m_0/\epsilon)x}$. To summarize after normalization, we obtain the eigenfunction of the zero-energy eigenvalue in the form of a bound state:

$$\psi_0^{\mathrm{D},(1)}(x) := \langle x|\psi_{E_x=0}^{\mathrm{D},(1)}\rangle$$
$$= \sqrt{\frac{m_0}{2\epsilon}}\begin{pmatrix} 1 \\ 1 \end{pmatrix}e^{-m_0|x|/\epsilon}. \tag{A45}$$

Let us next find a scattering state, with an incoming wave proportional to $Ae^{ik_x x}$ for $x < 0$, a reflection wave proportional to $Be^{-ik_x x}$ for $x < 0$, and a transmission wave proportional to $Ce^{ik_x x}$ for $x > 0$, where $k_x > 0$. For the incoming wave for $x < 0$, the eigenvalue problem (A37) reads

$$\begin{pmatrix} \epsilon k_y & im_0 \\ -im_0 & -\epsilon k_y \end{pmatrix}\begin{pmatrix} \psi_1 \\ \psi_2 \end{pmatrix} = E_x\begin{pmatrix} \psi_1 \\ \psi_2 \end{pmatrix}, \tag{A46}$$
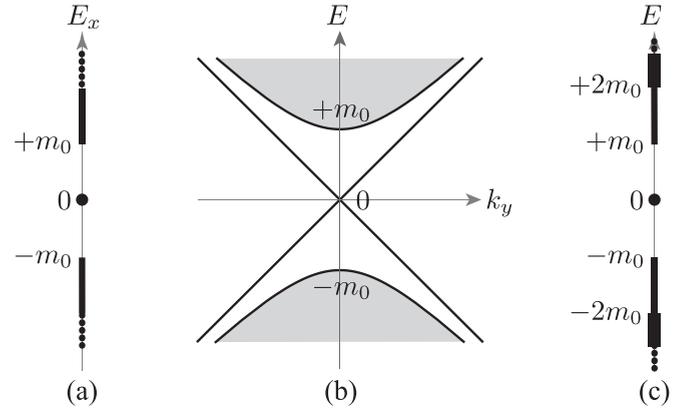

FIG. 8. (a) The energy spectrum of the 1D Dirac Hamiltonian with a domain wall in the mass term. (b) The dispersion relation of our 2D extended Dirac Hamiltonian with a domain wall only in the mass term $m_x(x)$, whereas $m_y(y) \equiv 0$. (c) The energy spectrum of our 2D extended Dirac Hamiltonian with domain walls in both the mass terms $m_x(x)$ and $m_y(y)$.

which yields

$$\big|\psi_{E_x}^{\mathrm{D},(1)}\big\rangle = \begin{cases} \begin{pmatrix} i\cos\varphi \\ \sin\varphi \end{pmatrix} & \text{for } E_x = +\sqrt{(\epsilon k_x)^2 + m_0^2}, \\ \begin{pmatrix} -i\sin\varphi \\ \cos\varphi \end{pmatrix} & \text{for } E_x = -\sqrt{(\epsilon k_x)^2 + m_0^2}, \end{cases} \tag{A47}$$

where the coefficient φ is defined in

$$\tan 2\varphi = \frac{m_0}{\epsilon k_y}. \tag{A48}$$

Let us hereafter focus on the scattering state with the positive energy eigenvalue $E_x = +\sqrt{(\epsilon k_x)^2 + m_0^2}$. We therefore assume the incoming wave of the form

$$Ae^{ik_x x}\begin{pmatrix} i\cos\varphi \\ \sin\varphi \end{pmatrix} \tag{A49}$$

for $x < 0$. Similarly, the reflection wave is given by

$$Be^{-ik_x x}\begin{pmatrix} i\sin\varphi \\ \cos\varphi \end{pmatrix} \tag{A50}$$

for $x < 0$, while the transmission wave is given by

$$Ce^{ik_x x}\begin{pmatrix} -i\cos\varphi \\ \sin\varphi \end{pmatrix} \tag{A51}$$

for $x > 0$. In order for the first two on the left and the last on the right to be continuous at the origin, the amplitudes must satisfy

$$A\cos\varphi + B\sin\varphi = -C\cos\varphi, \tag{A52}$$

$$A\sin\varphi + B\cos\varphi = C\sin\varphi. \tag{A53}$$

They are followed by

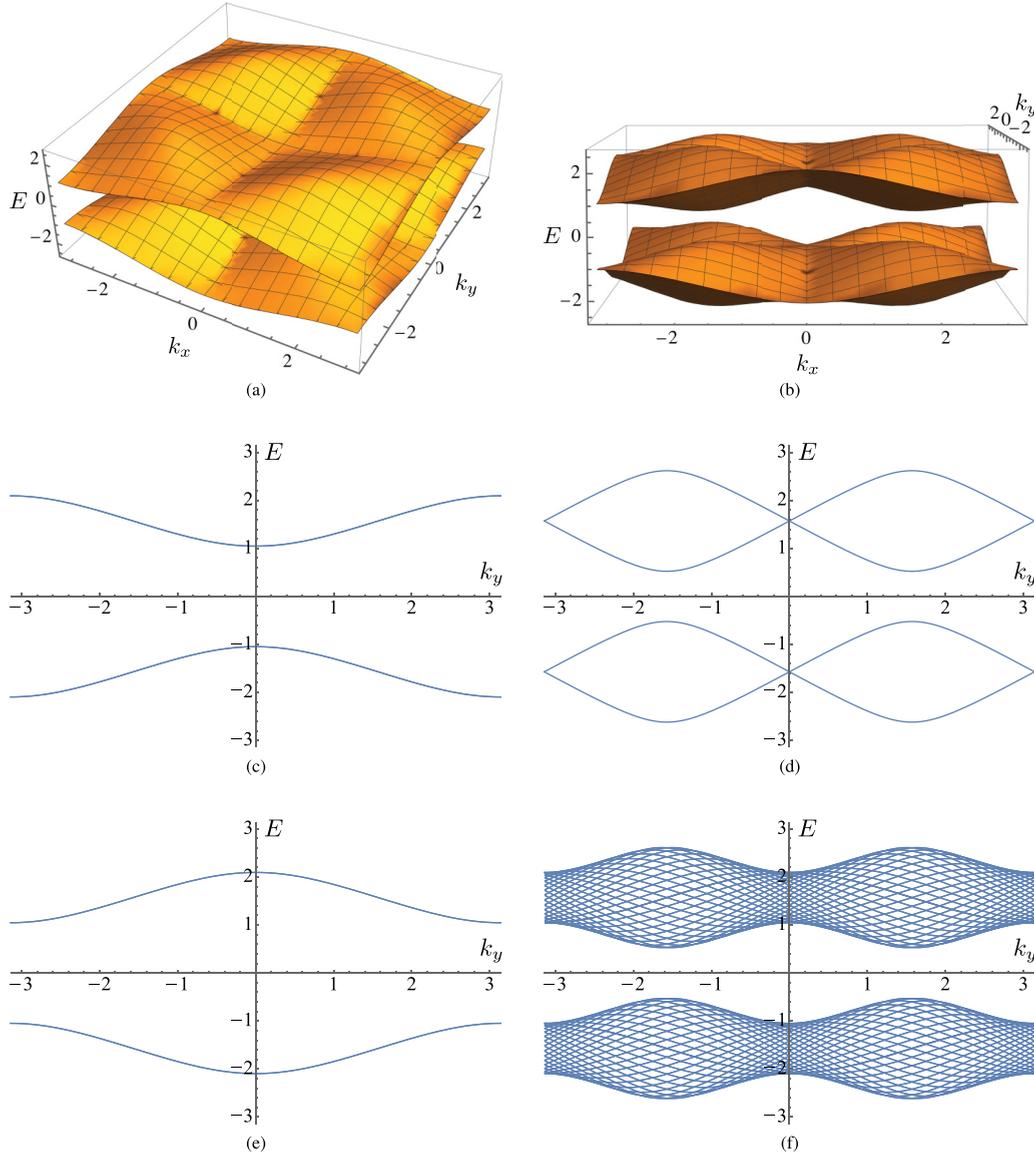$$B = -A\sin 2\varphi, \tag{A54}$$

$$C = -A\cos 2\varphi, \tag{A55}$$

FIG. 9. Band structure for $\theta_x = \pi/3$ and $\theta_y = 0$. (a) and (b) Energy bands from two different viewpoints. (c), (d), and (e) Cross sections of the bands at $k_x = 0$, $k_x = \pi/2$, and $k_x = \pi$, respectively. (f) Projection of the bands over the k_x axis onto the k_y axis. We set $\hbar = a = \Delta t = 1$.

which indeed satisfy the flux conservation $k_x|A|^2 = k_x|B|^2 + k_x|C|^2$. We can similarly find a solution for the negative energy eigenvalue $E_x = -\sqrt{(\epsilon k_x)^2 + m_0{}^2}$.

We thereby conclude that the scattering states have the energy continua of the forms $E_x = \pm\sqrt{(\epsilon k_x)^2 + m_0{}^2}$ with the energy gap $-m_0 < E_x < m_0$, in the middle of which exists the point-spectral bound state of the zero-energy eigenvalue; see Fig. 8(a). This implies that the bound state is actually a topological edge state.

b. First-order topological edge states in 2D

We now find the eigenspectrum of our 2D extended Dirac Hamiltonian (1) but with $m_y(y) \equiv 0$. This corresponds to the situation of 2D DTQW in Sec. II B.

Following the general formulation in Appendix A 1 again, we can find the eigenstates of $H_D^{(2)}$ out of the eigenstates of H_{D_x} and H_{D_y}. For H_{D_x}, we set the domain wall (A38), and

hence its eigenstates are the ones given in Appendix A 3 a, namely the topological edge state (A45) with a point spectrum $E_x = 0$ and the scattering states (A49)–(A51) with the energy continuum $E_x = \pm\sqrt{(\epsilon k_x)^2 + m_0{}^2}$. For H_{D_y}, on the other hand, we have only the kinetic term $\epsilon p_y \sigma_x \otimes \tau_z$, and therefore the eigenvalues have the linear dispersions $E_y = \pm\epsilon k_y$ for the eigenvectors

$$\frac{1}{\sqrt{2}}\begin{pmatrix}1\\\pm1\end{pmatrix} \otimes \begin{pmatrix}e^{\pm ik_yy}\\0\end{pmatrix} \quad \text{and} \quad \frac{1}{\sqrt{2}}\begin{pmatrix}1\\\pm1\end{pmatrix} \otimes \begin{pmatrix}0\\e^{\pm ik_yy}\end{pmatrix}. \tag{A56}$$

We now combine the eigenvalues of the two Hamiltonians as in Eq. (A17). Combining the point spectrum $E_x = 0$ and the linear dispersions $E_y = \pm\epsilon k_y$ produces $E = \pm\epsilon k_y$. Combining the continuum with the linear dispersions gives

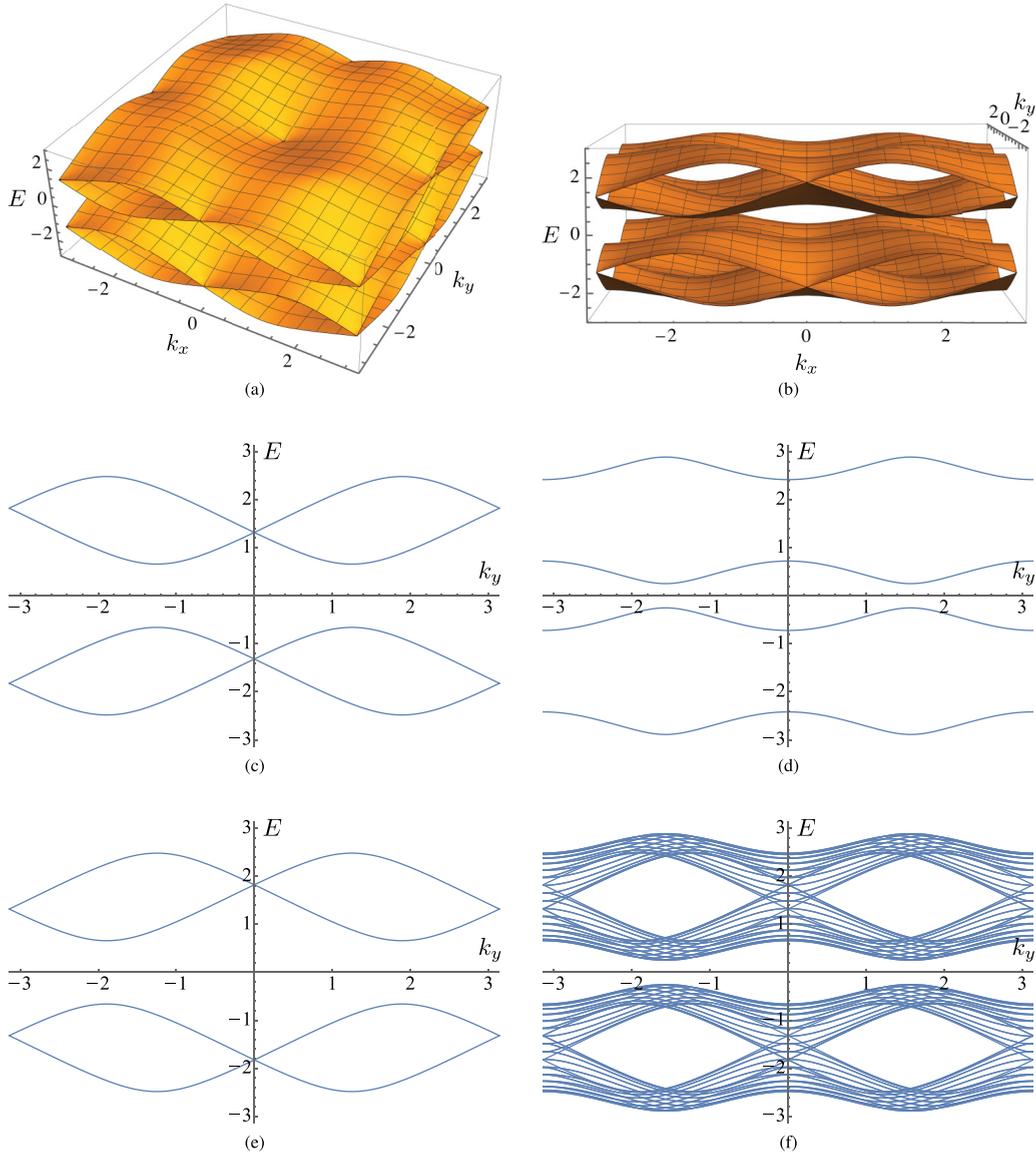$$E = \pm\sqrt{(\epsilon k_x)^2 + (\epsilon k_y)^2 + m_0{}^2}. \tag{A57}$$

FIG. 10. Band structure for $\theta_x = \pi/3$ and $\theta_y = \pi/3$. (a) and (b) Energy bands from two different viewpoints. (c), (d), and (e) Cross sections of the bands at $k_x = 0$, $k_x = \pi/2$, and $k_x = \pi$, respectively. (f) Projection of the bands over the k_x axis onto the k_y axis. We set $\hbar = a = \Delta t = 1$.

When we plot these eigenvalues for k_y, the former is the linear dispersions while the latter is hyperbolic curves filled by scanning k_x; see Fig. 8(b). This describes the region near the origin of the energy spectrum in Fig. 2(a) within the Trotter approximation.

c. Higher-order topological corner state in 2D

We finally find the eigenspectrum of the 2D extended Dirac Hamiltonian (1) with domain walls both in x and y directions:

$$m_y(y) = \begin{cases} +m_0 & \text{for } y > 0, \\ -m_0 & \text{for } y < 0, \end{cases} \qquad (A58)$$

in addition to Eq. (A38). This corresponds to the situation of 2D DTQW in Sec. II C.

Both H_{D_x} and H_{D_y} now have the spectrum given in Appendix A 3 a. Combining them, we have the following four types of eigenvalues:

(i) $E_x = 0$ and $E_y = 0$ combine to produce $E = 0$. This zero-energy eigenstate will be identified below as a second-order topological corner state.

(ii) $E_x = \pm\sqrt{(\epsilon k_x)^2 + m_0^2}$ and $E_y = 0$ combine to produce $E = \pm\sqrt{(\epsilon k_x)^2 + m_0^2}$. This is an edge state (the first-order topological state) in the y direction, but a scattering state in the x direction. In other words, an edge continues in the x direction, localized in the y direction, on which a state propagates with the momentum k_x.

(iii) $E_x = 0$ and $E_y = \pm\sqrt{(\epsilon k_y)^2 + m_0^2}$ combine to produce $E = \pm\sqrt{(\epsilon k_y)^2 + m_0^2}$. In this case, an edge continues in the y direction, localized in the x direction, on which the state propagates with the momentum k_y.
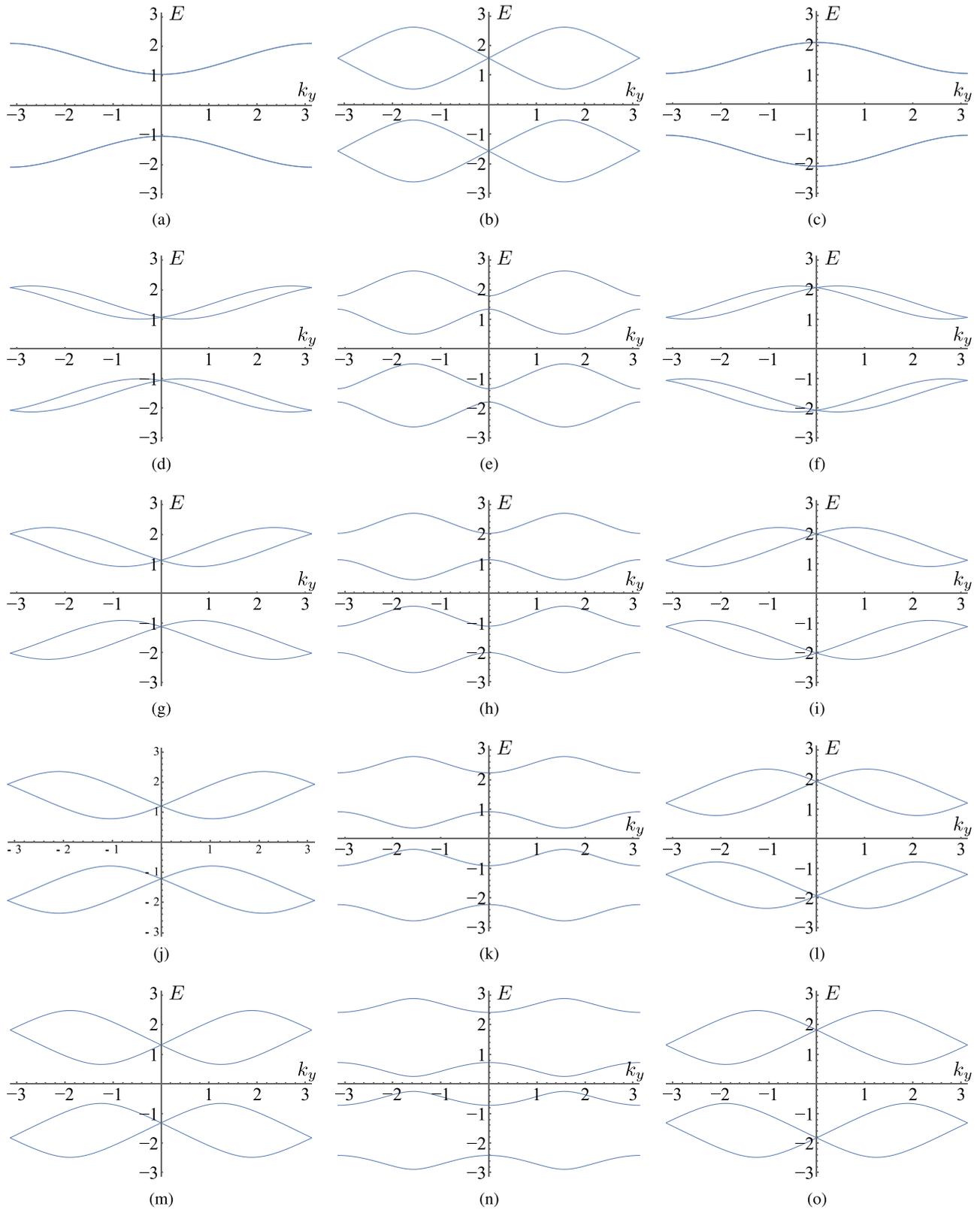
FIG. 11. Cross sections of the bands at $k_x = 0$, $k_x = \pi/2$, and $k_x = \pi$ on the first, second and third columns, respectively. We vary θ_y to 0, $\pi/12$, $\pi/6$, $\pi/4$, and $\pi/3$ on the five rows from top to bottom, respectively. We set $\hbar = a = \Delta t = 1$.

(iv) $E_x = \pm\sqrt{(\epsilon k_x)^2 + m_0{}^2}$ and $E_y = \pm\sqrt{(\epsilon k_y)^2 + m_0{}^2}$ combine to produce $E = \pm\sqrt{(\epsilon k_x)^2 + (\epsilon k_y)^2 + 2m_0{}^2}$. Here the state propagates both in the x and y directions.

We thereby find a zero-energy eigenvalue, the energy continua starting from $\pm m_0$, and the energy continua starting from $\pm 2m_0$; see Fig. 8(c).

We can find the zero-energy eigenfunction based on Eq. (A18). The zero-energy eigenfunction of H_{D_x} with Eq. (A38) takes the form of the bound state (A45) in the x direction and the one of H_{D_y} with Eq. (A58) takes the similar form of the bound state in the y direction. Multiplying them, we obtain the zero-energy eigenfunction of the 2D Hamiltonian in the form

$$
\begin{aligned}
\psi^{\mathrm{D},(2)}_{E=0}(x, y) &:= \langle x | \psi^{\mathrm{D},(1)}_{E_x=0} \rangle \langle y | \psi^{\mathrm{D},(1)}_{E_y=0} \rangle \\
&= \frac{m_0}{2\epsilon} \begin{pmatrix} 1 \\ 1 \end{pmatrix} \otimes \begin{pmatrix} 1 \\ 1 \end{pmatrix} \exp\left[-\frac{m_0}{\epsilon}(|x| + |y|) \right].
\end{aligned}
$$
(A59)

This has a peak in the xy plane because an edge state running in the x direction and the edge state running in the y direction were multiplied together, and hence it is identified as a second-order topological state, namely the corner state. This describes each peak that our 2D DTQW demonstrates in Fig. 6.

APPENDIX B: BAND STRUCTURE FOR FINITE θ_x AND θ_y

We here show the band structure for finite θ_x and θ_y. In the following, let us fix $\theta_x = \pi/3$ and vary θ_y from 0 to $\pi/3$.

The model generally has four bands. For $\theta_y = 0$, the first and second bands as well as the third and fourth bands are closed on the lines $k_x = 0, \pm\pi$ and $k_y = 0, \pm\pi$; see Fig. 9. When projected on the k_y axis, each of the upper and lower energy bands appears to be filled.

For $\theta_y = \pi/3$, on the other hand, all bands are open on the lines $k_x = 0, \pm\pi$ and $k_y = 0, \pm\pi$ except for the Dirac points $(k_x, k_y) = (0, 0), (\pm\pi/2, \pm\pi/2), (\pm\pi, \pm, \pi)$; see Fig. 10. When projected on the k_y axis, we can now see large openings in each of the upper and lower bands. When we introduce the effective potential

$$
\theta_x(x) = \begin{cases} -\pi/3 & \text{for } |x| > L_x/2, \\ \pi/3 & \text{for } |x| \leqslant L_x/2, \end{cases}
$$
(B1)

we see edge modes in the openings as in Fig. 7 of the main text.

Figure 11 shows the variation of the cross sections on $k_x = 0$, $k_x = \pi/2$ and $k_x = \pi$ for $\theta_y = 0, \pi/12, \pi/6, \pi/4, \pi/3$. We can see the openings at each cross section become wider as we increase θ_y.

[1] Y. Aharonov, L. Davidovich, and N. Zagury, Phys. Rev. A **48**, 1687 (1993).

[2] D. A. Meyer, J. Stat. Phys. **85**, 551 (1996).

[3] R. P. Feynman and A. R. Hibbs, *Quantum Mechanics and Path Integrals*, International Series in Pure and Applied Physics (McGraw-Hill, New York, 1965).

[4] E. Farhi and S. Gutmann, Phys. Rev. A **58**, 915 (1998).

[5] A. Ambainis, E. Bach, A. Nayak, A. Vishwanath, and J. Watrous, in *Proceedings of the Thirty-Third Annual ACM Symposium on Theory of Computing*, STOC '01 (Association for Computing Machinery, New York, 2001), pp. 37–49.

[6] R. Asaka, K. Sakai, and R. Yahagi, Quantum Sci. Technol. **6**, 035004 (2021).

[7] G. S. Engel, T. R. Calhoun, E. L. Read, T.-K. Ahn, T. Mančal, Y.-C. Cheng, R. E. Blankenship, and G. R. Fleming, Nature (London) **446**, 782 (2007).

[8] N. Dudhe, P. K. Sahoo, and C. Benjamin, Phys. Chem. Chem. Phys. **24**, 2601 (2022).

[9] T. Oka, N. Konno, R. Arita, and H. Aoki, Phys. Rev. Lett. **94**, 100602 (2005).

[10] T. Kitagawa, M. S. Rudner, E. Berg, and E. Demler, Phys. Rev. A **82**, 033429 (2010).

[11] T. Kitagawa, Quantum Inf. Process. **11**, 1107 (2012).

[12] J. K. Asbóth and H. Obuse, Phys. Rev. B **88**, 121406(R) (2013).

[13] F. W. Strauch, Phys. Rev. A **73**, 054302 (2006).

[14] C. Di Franco, M. Mc Gettrick, and T. Busch, Phys. Rev. Lett. **106**, 080502 (2011).

[15] L. A. Bru, G. J. de Valcárcel, G. Di Molfetta, A. Pérez, E. Roldán, and F. Silva, Phys. Rev. A **94**, 032328 (2016).

[16] P. Arrighi, G. Di Molfetta, I. Márquez-Martín, and A. Pérez, Phys. Rev. A **97**, 062111 (2018).

[17] A. Murani, A. Kasumov, S. Sengupta, Y. A. Kasumov, V. T. Volkov, I. I. Khodos, F. Brisset, R. Delagrange, A. Chepelianskii, R. Deblock, H. Bouchiat, and S. Guéron, Nat. Commun. **8**, 15941 (2017).

[18] S. Imhof, C. Berger, F. Bayer, J. Brehm, L. W. Molenkamp, T. Kiessling, F. Schindler, C. H. Lee, M. Greiter, T. Neupert, and R. Thomale, Nat. Phys. **14**, 925 (2018).

[19] C. W. Peterson, W. A. Benalcazar, T. L. Hughes, and G. Bahl, Nature (London) **555**, 346 (2018).

[20] L. H. Ryder, *Quantum Field Theory*, 2nd ed. (Cambridge University Press, Cambridge, 1996).

[21] W. A. Benalcazar, B. A. Bernevig, and T. L. Hughes, Science **357**, 61 (2017).

[22] S. Hayashi, Commun. Math. Phys. **364**, 343 (2018).

[23] F. Schindler, A. M. Cook, M. G. Vergniory, Z. Wang, S. S. P. Parkin, B. A. Bernevig, and T. Neupert, Sci. Adv. **4**, eaat03 (2018).

[24] J. Langbehn, Y. Peng, L. Trifunovic, F. von Oppen, and P. W. Brouwer, Phys. Rev. Lett. **119**, 246401 (2017).

[25] Z. Song, Z. Fang, and C. Fang, Phys. Rev. Lett. **119**, 246402 (2017).

[26] W. A. Benalcazar, B. A. Bernevig, and T. L. Hughes, Phys. Rev. B **96**, 245115 (2017).

[27] R. Jackiw and C. Rebbi, Phys. Rev. D **13**, 3398 (1976).

[28] N. Shenvi, J. Kempe, and K. Birgitta Whaley, Phys. Rev. A **67**, 052307 (2003).

[29] M. Yamagishi, N. Hatano, and O. Hideaki, Defining a quantum active particle using non-Hermitian quantum walk (unpublished).

[30] F. Schweitzer, W. Ebeling, and B. Tilch, Phys. Rev. Lett. **80**, 5044 (1998).

[31] S.-Q. Shen, *Topological insulators*, 2013 ed., Springer Series in Solid-State Sciences (Springer, Berlin, 2013).

[32] A. Kitaev, in *Advances in Theoretical Physics: Landau Memorial Conference, 22–26 June 2008, Chernogolokova, Russia*, edited by V. Lebedev and M. Feigel'man, AIP Conf. Proc. No. 1134 (AIP, New York, 2009), p. 22.

[33] S. Ryu, A. P. Schnyder, A. Furusaki, and A. W. W. Ludwig, New J. Phys. **12**, 065010 (2010).

[34] Y. Yoshimura, S. Hayashi, K.-I. Imura, and T. Nakanishi, Bulk-edge-corner correspondence at an arbitrary angle (unpublished).